THE 24th INTERNATIONAL MEETING ON REDUCED ENRICHMENT FOR RESEARCH AND TEST REACTORS

San Carlos de Bariloche, Argentina
November 3-8, 2002

ATOMISTIC MODELLING OF THE INTERDIFFUSION OF Al IN THE UMo BASED FUEL

Jorge E. Garcés [a,b], Armando C. Marino [a] and Guillermo Bozzolo [b,c]

[a] Centro Atómico Bariloche, Comisión Nacional de Energía Atómica, 8400 Bariloche, Argentina
[b] Ohio Aerospace Institute, 22800 Cedar Point Rd., Cleveland, OH 44142, USA
[c] NASA Glenn Research Center, Cleveland, OH 44135, USA

ATOMISTIC MODELLING OF THE INTERDIFFUSION OF Al IN THE UMo BASED FUEL

Jorge E. Garcés [a,b], Armando C. Marino [a] and Guillermo Bozzolo [b,c]

[a] Centro Atómico Bariloche, Comisión Nacional de Energía Atómica, 8400 Bariloche, Argentina
[b] Ohio Aerospace Institute, 22800 Cedar Point Rd., Cleveland, OH 44142, USA
[c] NASA Glenn Research Center, Cleveland, OH 44135, USA

ABSTRACT

The analysis of the initial stages and trends in the process of interdiffusion of Al in the UMo solid solution as a function of Mo concentration is made using the BFS method for alloys. The approach presented in this work helps to understand the exchange mechanism between adatoms and substrate atoms in the binary systems, leading to the behavior observed in the ternary Al-U-Mo system. While in Al/U Al atoms show a noticeable tendency to interdiffusion in the bulk, in Al/Mo the same atoms show a tendency to layer-by-layer growth and the formation of structures in the overlayer. In the case of Al/U-Mo, the two competing behaviors observed for Al/Mo and Al/U, translate into the role of regions rich in Mo acting as interdiffusion barriers, in excellent agreement with experimental evidence.

1. INTRODUCTION

The development of high density U-alloys with an increased concentration of U is one of the key problems for developing high neutron flux research reactors with low enrichment uranium fuel [1]. The U-Mo alloy system is one of the possible candidates because a solid solution of Mo in bcc-U has acceptable irradiation properties for reactor fuels. However, several basic issues must be addressed in order to have a better understanding of the fundamental behavior of this fuel. In this sense, the processes involved in the interaction between the aluminum matrix and the UMo solid solution are of particular importance, as interdiffusion or interfacial reaction in the Al/UMo composite, with considerable volume increase for low Mo composition, has been found. This process can impact the performance of nuclear fuel materials. Other basic questions relate to the role of new additives in the stability of the bcc phase as well as in the improvement of the thermal compatibility with the Al matrix.

The answers to these questions could arise from experiment, theory, or from a combination of both approaches. The method for developing or improving specific alloys has been mostly based on extensive experimental trial and error work, which is both expensive and time-consuming. Recently, however, the increasing role of computational modeling in the development of structural materials has become a valuable tool to aid the experimental work. If theoretical modelling could also be included in the development of nuclear fuels, then the experimental process could be better oriented and, as a consequence, the number of experiments could be reduced to specific ones needed to verify the theoretical predictions. While the virtual design of new materials through complex computer simulations is still many years away, its success will depend on the availability of a unified approach that provides the same level of simplicity and accuracy for any possible application, whether it is directed to surface and/or bulk analysis. Although first-principles approaches provide the most accurate framework for such studies, the complexity of the problems at hand and their substantial computational requirements impose limitations that still prevent these approaches from becoming economical predictive tools. In fact, the theoretical description of actinide metals and their alloys poses a severe challenge to modern electronic-structure theory [2] and has eluded accurate treatment by semiempirical or quantum approximate methods (QAM's)

as well. As a consequence, theoretical modelling efforts to describe the complex behavior observed experimentally in these systems have been limited, both in number and scope.

The tendency to incorporate atomistic simulations as a standard tool in the analysis of complex systems has imposed high expectations on the range of applicability of theoretical methods and QAM's, their computational efficiency, their ease of implementation, and the type of output that they provide. The purpose of the QAM's is to provide an efficient and accurate way to compute the total energy of arbitrary atomic systems in term of their geometrical configuration. Almost independently of their foundation and formulation, these methods rely on simplifications which, as a result, inevitably require the introduction of parameters. The recent trend of combining first-principles with QAM's has created new possibilities in the field of atomistic simulations, as they provide accurate and valuable input for the determination of these parameters when experiments are not available. In most cases, the existing QAM's are restricted to a few systems for which a specific (and therefore nontransferable) parameterization is developed, thus limiting their use. Additional restrictions generally apply, resulting in limitations on the efficiency or accuracy of the method in terms of type of lattice structure, number and type of element. One of these QAM's, the Bozzolo-Ferrante-Smith (BFS) method for alloys [3], is built on the basis of completely transferable parameters and can deal with complex systems and geometries, as it has no theoretical constraints regarding the type and number of elements, or on the number or type of phases it can handle. This method has been proven to be highly effective to study multicomponent systems [4] or surface alloys [5] but has never been applied to the study of an actinide-based multicomponent alloy.

The purpose of this work is to introduce atomistic modelling to understand the interdiffusion of Al along the grain boundaries of the U-Mo solid solution. We present preliminary results of a modelling effort dealing with the interdiffusion of Al in the (100) and (110) surfaces of a bcc-based U-Mo solid solution. The method was applied first to the deposition of Al in the (100) and (110) surfaces of Mo and U substrates. The results for the ternary system are discussed within the framework of the results obtained for the binary cases, Al/Mo and Al/U. Besides the fundamental features identified in these cases, the full ternary Al-U-Mo system is analyzed and its behavior compared with the experimental observations [6].

2. THE BFS METHOD

The BFS method has been applied to a variety of problems, ranging from bulk properties of solid solution fcc alloys [7] and the defect structure in ordered bcc alloys [8,9], to more specific applications including detailed studies of the structure and composition of alloy surfaces and surface alloys [5] or the determination of site subsitution preference in ordered ternary, quaternary and pentalloy B2 phase based compounds [4,10].

The BFS method overcomes the difficulties shared by other QAM's mentioned previously simply because of its interpretation and modelling of the alloy formation process [3]. In this method, any given system, regardless of its composition and structure, is always modelled in terms of two independent virtual processes which, properly coupled, are meant to result in the final state that is being studied. One of these virtual processes relates to the structural changes in the environment of any given atom (strain), and it consists of defining, for every atom, a virtual (perfect) monatomic equivalent crystal of its own species in a state of isotropic compression or expansion with respect to equilibrium. The amount of compression or expansion is defined so that the electron density in the vicinity of the atom in the real crystal resembles, in average, the corresponding one in the expanded or compressed perfect equivalent crystal [11]. The availability of a universal binding energy relationship (UBER) [12] to describe such isotropic transformations ensures an accurate and energetically correct description of the process, particularly for small departures from equilibrium. The other virtual process accounts for changes in the chemical environment of that same atom (chemical). Once again, another virtual perfect crystal, in a state of isotropic compression or expansion, is assigned. To properly decouple structural and chemical effects, it is necessary to introduce additional restrictions in the definition of these processes. In the first case, all atoms surrounding a given reference atom are considered as being of the same atomic species as the reference atom, thus freezing compositional degrees of freedom in the determination of the equivalent crystal

associated with structural changes. In the second case, the surrounding atoms retain their chemical identity, but are forced to occupy equilibrium lattice sites of a lattice characteristic of the reference atom. Both processes share one particular feature: any system is described in the same way, i.e., by means of virtual, ideal bulk crystals. As a result, whether the system involves the presence of surfaces or other extended defects, or a varying chemical composition, etc., the modelling of the formation process is done by means of these virtual crystals which, in their definition (their composition and structure), account for the particular features of the real system that they represent. Thus, the environment seen by an atom in the real crystal is translated into an equivalent, perfect crystal. The parameters used in the BFS method describe the virtual processes and the properties of these virtual crystals. As such, they are somewhat blind to the otherwise different systems that they describe, as they are always applied to the energetics of perfect, virtual, bulk crystals. In all cases they describe deviations from an equilibrium state of the equivalent crystal, thus eliminating a direct correlation with the nature of the actual situation which they are meant to represent. For example, the formation of a single vacancy is, in terms of the parameters used, no different from the substitution of a neighboring atom for one of a different species, or a surface defect. Therefore, it is expected that if the theory allows for an unequivocal definition of these virtual crystals, properly endowed with the necessary information on the real crystals that they represent, the parameters will then have the same level of reliability, or be able to extract the same amount and quality of information via the equations of the method, in any kind of situation.

It is also worth noting that the parameterization of the BFS method implies a somewhat different approach for the interaction between different atoms. In general, most approaches deal with this issue by introducing some sort of interaction potential with any parameter describing each constituent remaining unchanged. In BFS, it is precisely the set of parameters describing the pure element what is perturbed in order to account for the distortions introduced by the nearby presence of a different element or defect. In doing so, an additional advantage is thus introduced in the methodology, as the number of parameters is reduced to a minimum and their transferability is therefore guaranteed. It is, however, an additional burden on the method, as too much critical information must then be carried by a very small number of parameters. From a practical standpoint, however, it is obviously a matter of balance between the advantages and disadvantages that ultimately translates into an efficient and accurate method with a maximum range of applicability.

Basically, the BFS method provides a simple algorithm for the calculation of the energy of formation ΔH of an arbitrary alloy (the difference between the energy of the alloy and that of its individual constituents). In this method, the energy of formation is written as the superposition of elemental contributions of all the atoms in the alloy

$$\Delta H = \sum_i \varepsilon_i \tag{1}$$

For each atom, we partition the energy into two parts: a strain energy, ε_i^S, and a chemical energy, ε_i^C, contribution. By definition, the BFS strain and chemical energy contributions take into account different effects, i.e., geometry and composition, computing them as isolated effects. A coupling function, g_i, restores the relationship between the two terms. This factor is defined in such a way as to properly consider the asymptotic behavior of the chemical energy, where chemical effects are negligible for large separations between dissimilar atoms. A reference chemical energy, ε_i^{Co}, is also included to insure a complete decoupling of structural and chemical features. Summarizing, the contribution to the energy of formation of atom *i* is then

$$\varepsilon_i = \varepsilon_i^S + g_i \left(\varepsilon_i^C - \varepsilon_i^{Co}\right) \tag{2}$$

In what follows, we provide the basic operational equations needed to compute each one of the terms introduced above. The BFS strain energy, ε_i^S, differs from the commonly defined strain energy in that the actual chemical environment is replaced by that of a monatomic crystal. Its calculation is then

straightforward, even amenable to first-principles techniques. In this work we use Equivalent Crystal Theory (ECT) [11] for its computation due to its proven ability to provide accurate and computationally economical answers to most general situations. In all cases considered in this work, a rigorous application of ECT is reduced to that of its two leading terms, which describe average density contributions and bond-compression anisotropy. We neglect the three- and four-body terms dealing with the bond angle and face-diagonal anisotropies. The BFS strain energy contribution, ε_i^S, is obtained by solving the ECT perturbation equation

$$N R_1^{p_i} \exp^{-\alpha_i R_1} + M R_2^{p_i} \exp^{-(\alpha_i + 1/\lambda_i) R_2} = \sum_j r_j^{p_j} \exp^{-(\alpha_j + S(r_j)) r_j} \tag{3}$$

where N and M are the number of nearest- and next-nearest neighbors at distances R1 and R2, respectively, and where p, *l*, α and λ are ECT parameters that describe element *i* (see Ref. 11 for definitions and details), *r* denotes the distance between the reference atom and its neighbors, S(*r*) describes a screening function and the sum runs over nearest- and next-nearest-neighbors. This equation determines the lattice parameter a_i^S of a perfect crystal where the reference atom *i* has the same energy as it has in the geometrical environment of the alloy under study.

Once the lattice parameters of the (strain) equivalent crystal, a_i^S, is determined, the BFS strain energy contribution is computed using the universal binding energy relation of Rose et al. [12], which contains all the relevant information concerning a single-component system:

$$\varepsilon_i^S = E_i^C \left(1 - \left(1 + a_i^{S*} \right) \exp\left(- a_i^{S*} \right) \right) \tag{4}$$

where $\boldsymbol{E_i^C}$ is the cohesive energy of atom *i* and where the scaled lattice parameter $\boldsymbol{a_i^{S*}}$ is given by

$$a_i^{S*} = q\left(a_i^S - a_i^e \right) / l_i \tag{5}$$

where q is the ratio between the equilibrium Wigner-Seitz radius and the equilibrium lattice parameter $\boldsymbol{a_i^e}$.

The BFS chemical energy is obtained by a similar procedure. As opposed to the strain energy term, the surrounding atoms retain their chemical identity, but are forced to be in equilibrium lattice sites of an equilibrium crystal *i*. The BFS equation for the chemical energy is given by

$$N R_1^{p_i} \exp^{-\alpha_i R_1} + M R_2^{p_i} \exp^{-(\alpha_i + 1/\lambda_i) R_2} = \sum_j \left(N_{ik} r_1^{p_i} e^{-\alpha_{ik} r_1} + M_{ik} r_2^{p_i} e^{-(\alpha_{ki} + 1/\lambda_i) r_2} \right) \tag{6}$$

where N_{ik} and M_{ik} are the number of nearest- and next-nearest-neighbors of species *k* of atom *i*.

The chemical environment surrounding atom *i* is reflected in the parameter Δ_{ki}, given by

$$\alpha_{ik} = \alpha_i + \Delta_{ki} \tag{7}$$

where the BFS parameter Δ_{ki} (a perturbation on the single-element ECT parameter α_i) describe the changes of the wave function in the overlap region between atoms *i* and *k*. Once Eq. (6) is solved for the equivalent chemical lattice parameter a_i^c, the BFS chemical energy is then

$$\varepsilon_i^C = E_i^C \left(1 - \left(1 + a_i^{C*} \right) \exp\left(- a_i^{C*} \right) \right) \tag{8}$$

where $\gamma_i = 1$ if $a_i^{C*} > 0$ and $\gamma_i = -1$ if $a_i^{C*} < 0$, and the scaled chemical lattice parameter is given by

$$a_i^{C*} = q\left(a_i^C - a_i^e \right) / l_i \tag{9}$$

Finally, as mentioned above, the BFS strain and chemical energy contributions are linked by a coupling function g_i, which describes the influence of the geometrical distribution of the surrounding atoms in relation to the chemical effects and is given by

$$g_i = \exp\left(-a_i^{S*} \right) \tag{10}$$

The computation of ε_i^S and ε_i^C, using ECT [11], involves three pure element properties for atoms of species i: cohesive energy, lattice parameter and bulk modulus. The chemical energy, ε_i^C, includes two BFS perturbative parameters (Δ_{ki} and Δ_{ik}, with i, k = Al, U, Mo). In this work, all the necessary parameters were determined using the linearized augmented plane wave method (LAPW) [13], by computing the equilibrium properties of Al, Mo, and U in the bcc phase, as well as the equilibrium properties of AlMo, UMo and AlU ordered alloys in the B2 phase. All the calculations for pure elements and their alloys were performed using the generalized gradient approximation (GGA) for the exchange-correlation energy functional [14]. Table I lists the single element parameters. Table II lists the BFS parameters needed for applying the BFS method to the Al-U-Mo system.

	Lattice parameter (Å)	***Cohesive energy (eV)***	***Bulk Modulus (GPa)***	***p***	***α(Å^{-1})***	***l(Å)***	***λ(Å)***
Al	3.2381	3.44	69.14	4	1.7639	1.7639	1.0232
Mo	3.1616	6.67	260.61	8	3.4773	0.2641	0.7422
U	3.4501	5.55	141.40	12	4.8689	0.3132	0.8801

Table I: LAPW results for the lattice parameter, cohesive energy, and bulk modulus for the bcc phases of Al, Mo, and U. The resulting ECT [11] parameters p, α , l and λ are also listed (see text for their definition).

i/j	**Al**	**Mo**	**U**
Al		-0.03351	0.15351
Mo	0.10065		-0.06189
U	-0.03909	0.09261	

Table II: BFS parameters Δ_{ij} (in Å^{-1}) for all the binary combinations (i,j) of Al, Mo, and U.

3. RESULTS AND DISCUSSION

The BFS-based methodology, used to provide detailed insight on different aspects of bulk or surface alloys properties, assumes no *a priori* information on the system at hand and none of the experimental information is used in the formulation and application of the method. The only input necessary consists of the basic parameterization of the participating elements and lattice structures.

The basic procedure is based on the idea of generating catalogues of possible configurations suited to answer specific questions regarding the process of bulk or surface alloy formation. Then, the energy of these configurations is computed using the BFS method for alloys and plotted in the form of an energy

level spectrum. Each level in the spectrum is labelled by its difference in energy ΔE with respect to the lowest state in the set and by a shorthand notation indicating the type of structure that it represents. X(O) denotes an atom of species X in the overlayer O, X(S) in the surface, X(1b) one plane below the surface, X(2b) two planes below, etc. A subindex n(near) or f(far) denotes the distance between two atoms. A subindex [hkl] indicates the growing direction chosen by the atoms preceding the subindex. For simplicity, in this work we restrict our calculations to zero temperature and we disallow individual or collective relaxations. While it is true that the system at T = 0 K will reach the lowest energy states, it is also true that metastable states will have a role in determining the behavior of the system, i.e. the closer these states are to the ground state, the greater the likelihood that these states have of appearing in the actual system at finite temperature.

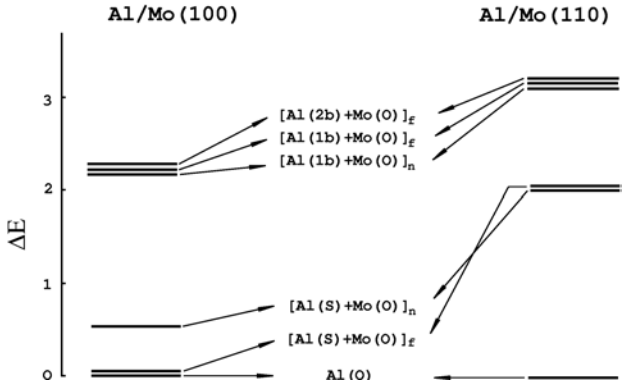

Fig. 1: Energy level spectrum for Al deposition on Mo. The figure shows results for the $N_{Al} = 1$ case listing, for each configuration and for each Mo crystal face, the difference in energy (in eV/atom) with respect to the lowest energy state (bottom). The adatom can either be located in the overlayer (O), in a surface site (S), in the first layer(1b) below the surface and two layers (2b) below the surface.

The purpose of this work is to apply this approach to the study of the deposition of Al on the (100) and (110) surfaces of the bcc-based U-Mo solid solution with the intent of not only reproducing the experimental results, but also finding the driving mechanism for the difference in behavior observed for different coverages in this system. While the experimental results show a large volume change for low Mo concentration in the solid solution, no significant dimensional changes are observed for a concentration of 10 wt % Mo [6]. For that purpose, we will apply the basic methodology outlined above to study the low coverage deposition of Al on the surface (100) and (110) of Mo and U, and Mo deposition on the same faces of U. Later, we will concentrate in the ternary system, i.e., the deposition of Al on the (100) and (110) surfaces of the U-Mo solid solution, to study the influence of the Mo atoms in the behaviors identified in the deposition of Al in the U(100) and U(110) slabs.

3.1. Al deposition on Mo(100) and Mo(110)

Auger electron spectroscopy (AES), low energy electron diffraction (LEED), and electron energy loss spectroscopy (EELS) experiments [15] show that a layer-by-layer growth mechanism of the adsorbate is primary at room temperature in the Al/Mo(110) system. For coverage lower than 0.34 ML, the adsorbate forms as a two-dimensional gas on the surface. Al atoms occupy random positions on the surface, a behavior which is probably responsible for the appearance of the (1x1) pattern of the substrate. Most probably no surface alloys are formed though the possibility is not fully excluded [15].

The theoretical description of the deposition of Al on a Mo substrate can be easily studied by considering a few basic configurations where the Al atom occupies sites in the overlayer, surface, or planes immediately below the surface plane. Fig. 1 shows the results for such configurations, plotted as a function of increasing difference in energy with respect to the lowest energy state in the set. For Al/Mo(100), the sequence starts with the Al atom in the overlayer (Al(O)), followed by states describing the penetration of Al into the Mo slab: $[Al(S)+Mo(O)]_f$, where the ejected Mo(O) atom locates itself far from the surface Al atom Al(S); $[Al(S)+Mo(O)]_n$, where they locate themselves in nearest-neighbor sites; $[Al(1b)+Mo(O)]_n$, where the Al atom goes to a site in the first layer below the surface (1b) and the Mo(O) atom remains close, followed by a similar configuration where Mo(O) migrates somewhere else on the surface ($[Al(1b)+Mo(O)]_f$), and lastly, $[Al(2b)+Mo(O)]_f$, where the Al atom interdiffuses to the second layer below the surface (2b) in the Mo substrate. Fig. 1 also lists the corresponding results for Al deposition on Mo(110), which are essentially identical to the Mo(100) case. From the onset, it is clear that

there is no penetration or formation of an Al/Mo surface alloy. BFS results indicate that the formation of a surface alloy is more likely on the (100) than in the (110) face, due to the larger energy gap between states with Al(O) and Al(S) in the second case. In order to understand the type of Al growth in the overlayer we study the deposition of two Al atoms in Mo(100) and Mo(110). The corresponding energy spectra, with energies referenced to the lowest energy state, are shown in Figs. 2 and 3, respectively. The lowest energy state, in both surfaces, corresponds to one where the Al atoms locates themselves initiating a chain in overlayer sites along the compact direction (i.e., [100] for the (100) face and [111] for the (110) face). The fact that the first excited state corresponds to Al dispersed randomly in the overlayer could explain the appearance of the (1x1) pattern observed experimentally. We conclude the analysis for this coverage noting that the spectra shown in Figs. 2 and 3 still indicates that the formation of a surface alloy is clearly unfavorable, mainly for the (110) surface. As the coverage increases, the calculations show the same basic features observed for low coverage: the formation of Al(O) chains along the close-packed direction both for Mo(100) and Mo(110), in agreement with experimental results.

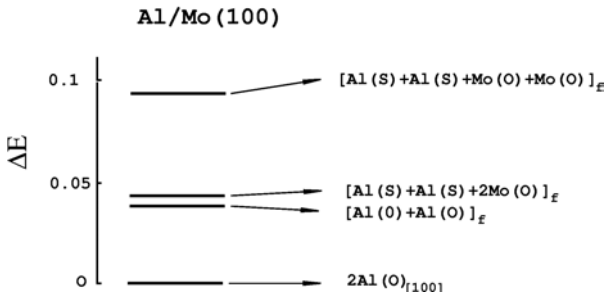

Fig. 2. Energy level spectrum for $N_{Al} = 2$ deposited on Mo(100) substrate. ΔE is the difference between the energy of formation per adatom (in eV/Atom) of each configuration and the lowest state.

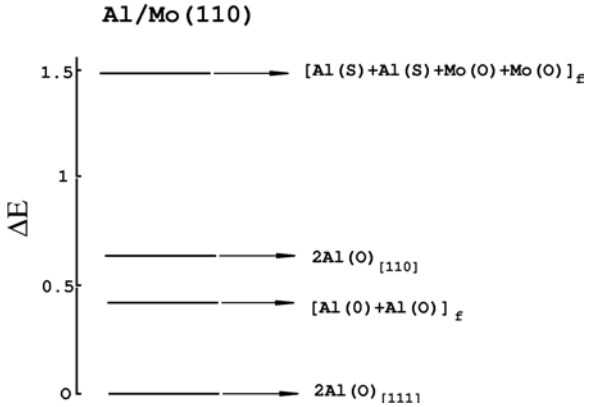

Fig. 3: Energy level spectrum for $N_{Al} = 2$ deposited on Mo(110) substrate. ΔE is the difference between the energy of formation per adatom (in eV/Atom) of each configuration and the lowest state.

3.2. Al deposition on U(100) and U(110)

In contrast with the behavior observed in Al/Mo, experimental observations indicate that there is strong interdiffusion of Al and intermetallic formation with different stoichiometry [6,16-18]. Fig. 4 summarizes the theoretical results for deposition of one single Al atom on a U(100) or U(110) slab. In both cases, the lowest energy state corresponds to Al in the bulk. The energy of the computational cell increases steadily as the Al atom approaches the surface, clearly indicating that Al has high solubility in U. Similar results are observed for two Al atoms, where the lowest energy state consists of two Al atoms in solution in the U bulk. There is, however, a close low energy state (0.03 eV/atom above the lowest energy configuration) where the two Al atoms are located at third neighbor distance. This can be seen as an emerging trend for ordering with increasing Al concentration. Further analysis of this feature, beyond the scope of this paper, will be performed in future efforts. As one last note on the Al/U system, it is interesting to point out that the (110) face of U inhibits the interdiffusion to deeper layers due to the large energy barrier (0.66 eV/atom) when an Al atom occupies a surface site. Once this energy barrier is overcome, the lowest energy state is again the configuration with the Al atom in the bulk.

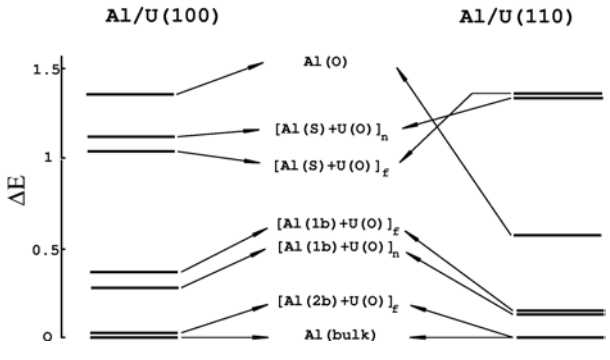

Fig. 4: Energy level spectrum for Al deposition on U for the (100) and (110) surfaces of U. The diagram shows the difference in energy (in eV/atom) with respect to the lowest energy state (bottom).

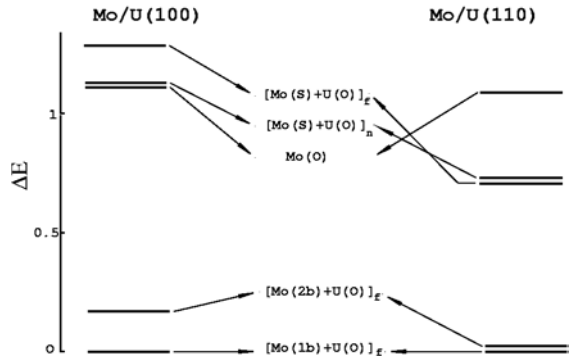

Fig. 5: Energy level spectrum for Mo deposition on U for the (100) and (110) surfaces of U. The diagram shows the difference in energy (in eV/atom) with respect to the lowest energy state (bottom)

3.3. Mo deposition on Mo(100) and Mo(110)

The deposition of Mo on U is, compared to the previous two cases, slightly more complex. The lowest energy state corresponds to the $[Mo(1b)+U(O)]_f$ case, followed by $[Mo(2b)+U(O)]_f$. These results, shown in Fig. 5, are consistent with the existence of a U-Mo solid solution, indicated by the preference of Mo for an U bulk-like environment. For U(100), the presence of a surface, however, triggers a segregation process by which the Mo atom migrates to layers in the sub-surface, but not to the actual surface plane, for which it has to overcome a small energy barrier (0.02 eV/atom). No such barrier exists in the U(110) case. Besides this single effect, there are minimal differences between the computed behavior in the (100) and (110) face of U.

3.4. Al deposition on the U-Mo solid solution

The results shown in Figs. 1-5 are, in all cases, in agreement with experiment. This is indicative of the robustness of the BFS parameters used to describe the interactions between the different pair combinations. Having raised the necessary confidence on this set of BFS parameters, we now apply them to the study of the ternary Al-U-Mo system

The experimental results show that the U 2 wt% Mo/Al dispersions increase in volume by 26% at 400 C after 2000 h. This large volume change is mainly due to the formation of voids and cracks resulting from nearly complete interdiffusion of U-Mo and Al. No significant dimensional change occurs in the U 10 wt% Mo/Al dispersions. Interdiffusion between U 10 wt% Mo and aluminum is found to be minimal. The different diffusion behavior is primarily due to the fact that U 10 wt% Mo particles are supersaturated with substitutional molybdenum, more so than with U 2 wt% Mo particles. Al diffuses into the U 2 wt% Mo particles relatively rapidly along grain boundary with nearly pure U forming UAl_3 almost fully throughout the 2000 h anneal, whereas the Mo supersaturated in the U 10 wt% Mo particles inhibit the diffusion of Al atoms [6].

We will model now the deposition of Al on a U-Mo substrate following the methodology applied to the binary systems. We first examine the deposition of a single Al atom on a U-Mo(100) substrate as a function of the distance between Al and Mo and as a function of the location of the Mo atom. For completeness, the corresponding results for U-Mo(110) are also shown.

The first case studied corresponds to the Mo atom located in a surface site: Mo(S). The results are shown in Fig. 6. In all cases the ejected U atom is deposited far from the Al or Mo atom. The lowest energy state for both crystal faces is [Al(2b)+Mo(S)]. This is true both for the case in which Mo(S) is close to or far from the deposited Al atom. Clearly, the presence of a single Mo atom, regardless of its location relative to the Al atom, does not change the trend observed for Al/U(100) or Al/U(110), where Al interdiffusion dominates. In the case when the Mo atom is located in a 1b site, [Mo(1b)+U(O)] [see Fig. 7], once again the lowest energy states are those where Al interdiffuses in the substrate with the Al and Mo atoms far from each other. The BFS results show that for the (110) face there is an energy barrier (0.34 eV/atom) that probably affects the interdiffusion of Al to deeper layers while no such barrier exists in the (100) face. Besides this effect, there are no substantial differences between the computed behavior in the (100) and (110) faces of the U-Mo solid solution.

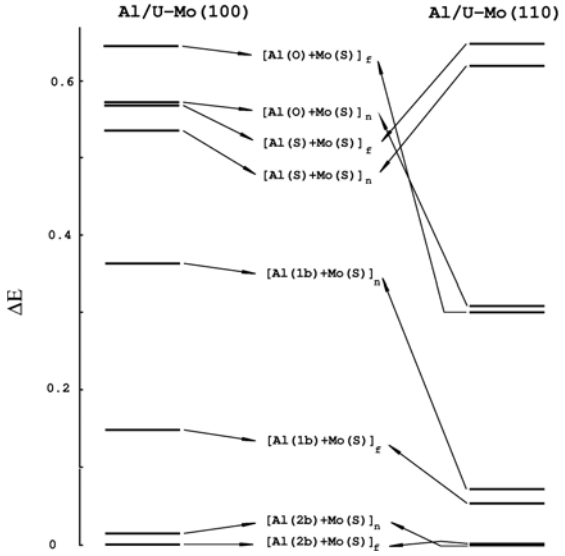

Fig. 6: Energy level spectra for Al deposition on a U slab in the presence of a Mo atom in a surface site. The configurations are ordered, top to bottom, in terms of decreasing difference in energy with the lowest energy state.

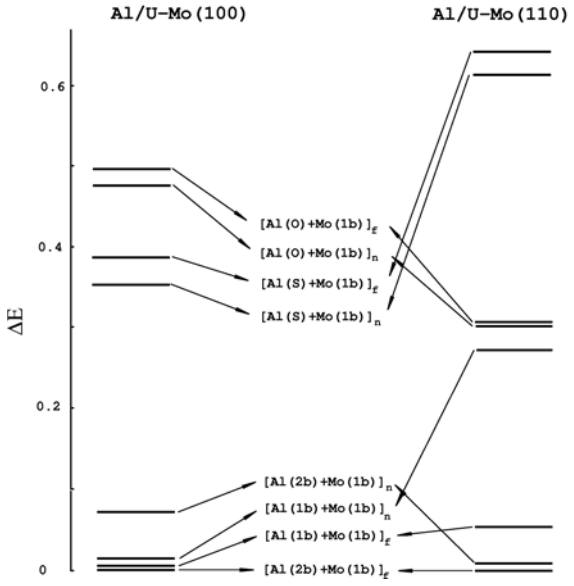

Fig. 7: Energy level spectra for Al deposition on a U slab in the presence of a Mo atom located in the plane below the surface (1b). The configurations are ordered, top to bottom, in terms of decreasing difference in energy with the lowest

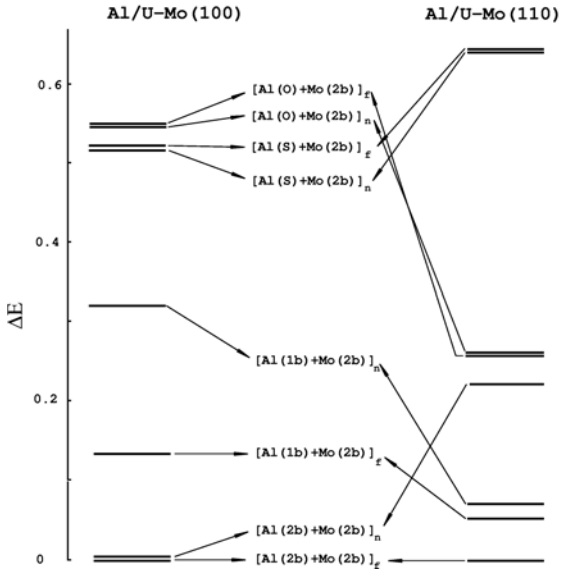

Fig. 8: Energy level spectra for Al deposition on a U slab in the presence of a Mo atom located in two planes below the surface (2b). The configurations are ordered, top to bottom, in terms of decreasing difference in energy with

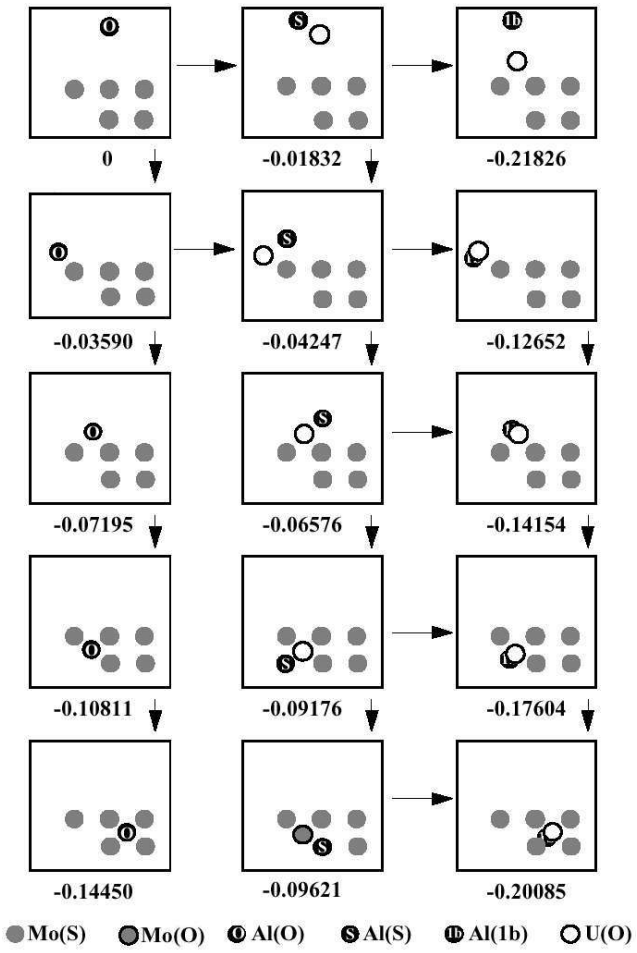

Fig. 9: Top view of different configurations showing an Al atom (black disk) in different overlayer (left column), surface (center column) and subsurface sites (right column) in the vicinity of a cluster of Mo atoms (gray disks) in an U substrate. Ejected U atoms are denoted with an open circle. Each configuration is labeled by the difference in energy (in eV/atom) with the reference state in which an Al adatom is located away from the Mo patch (top left corner). The horizontal or vertical arrows indicate those transitions that are energetically favored.

energy state.

the lowest energy state.

The results in Fig. 6 to Fig. 8 show that Al diffuses into the U-Mo substrate for both substrate terminations, in spite of the presence of an energy barrier when Al occupies surface sites, as seen in the (110) surface. However, a close examination of the magnitude of the energy gaps between the configurations whose ordering lead to this conclusion indicates that the interdiffusion of Al is facilitated in regions with low Mo concentration. In summary, the presence of Mo affects, but does not inhibit, Al interdiffusion in the bulk of U-Mo solid solution for this level of coverage, i.e., in the very dilute limit.

A better understanding of this behavior can be obtained by analyzing a set of configurations that model the penetration of Al into subsurface layers in regions of high Mo surface concentration. The fifteen configurations displayed in Fig. 9 describe the process in different ways: a) from top to bottom, showing the evolution of an Al atom in the overlayer (left column), surface layer (center column) and 1b layer (right column), in the presence of a cluster of Mo(S) atoms, and b) from left to right, showing the evolution of the Al atom as it moves from the overlayer site, to the surface site, and to the 1b layer. This is

shown for different locations of Al relative to the Mo(S) patch: far from the patch (top row), as a nearest-neighbor of a `corner' Mo(S) atom (second row), with two, three and four (third, fourth and fifth row, respectively) nearest-neighbors in the Mo patch.

The top row indicates that the penetration of Al (when deposited far from the Mo patch) in subsurface layers is energetically favored, an effect that is less pronounced as Al(O) approaches the Mo patch: the second row indicates that the process is still possible if Al(O) connects to the Mo(S) patch via one Mo(S) atom, but unlikely when the number of Al(O)-Mo(S) bonds increases (third, fourth, and fifth row). However, regardless of their proximity to the patch, Al atoms tend to migrate to Mo-rich regions. All three columns in Fig. 8 represent, from top to bottom, the process of Al diffusion towards the Mo patch. In all three cases, whether Al is in an overlayer, surface or 1b site, the lowest energy state is characterized by maximum coordination between the Al atom, the Mo patch and the surrounding U environment. This analysis shows that, in agreement with experiment, Al interdiffusion is prevalent in Mo-defficient regions of the U-Mo substrate.

4. CONCLUSIONS

In this work, the BFS method for alloys was applied to the atomistic modelling of Al interdiffusion in U-Mo as a function of Mo concentration. The simple BFS-based methodology presented in this work assumes no *a priori* information on the system at hand. The only input necessary consists of the basic parametrization of the participating elements and lattice structures. As a consequence, a much needed freedom in the analysis of nuclear materials is thus achieved. The method was applied first to the deposition of Al in the (100) and (110) surfaces of Mo and U substrates. Two opposite behaviors were found: while in Al/U Al atoms show a noticeable tendency to interdiffusion in the bulk, in Al/Mo the same atoms show a tendency to layer-by-layer growth and the formation of structures in the overlayer. In excellent agreement with experimental evidence, the atomistic modelling results show that these two opposite behaviors translate in the ternary system Al/U-Mo to Mo-rich regions acting as an interdiffusion barrier for Al atoms.

ACKNOWLEDGMENTS

Fruitful discussions with N. Bozzolo are gratefully acknowledged. Financial support for this work was provided by the International Computational Materials Science Consortium (OAI/NASA) and the HOTPC program at NASA Glenn Research Center, USA, and by the Comisión Nacional de Energía Atómica (CNEA), Argentina.

REFERENCES

[1] G.L. Hofman, L.C. Walters, in Nuclear Materials, vol. 10A, VCH, NY, 1994.
[2] M.D. Jones, J.C. Boettger, R.C. Albers, D.J. Singh, Phys. Rev. B 61 (2000) 4644.
[3] G. Bozzolo, J. Ferrante, E. D Noebe, F. Honecy, P. Abel, Comp. Mat. Sci. 15 (1999) 169.
[4] A. Wilson, G.Bozzolo, R.D.Noebe and J.W.Howe, Acta Mater. 50 (2002) 2787.
[5] *Atomistic modelling of surface alloys.* G. Bozzolo and J.Garcés, published in "Surface alloys and Alloys Surface", D.P. Woodruff, ed. Published in The Chemical Physics of Solid Surface, Vol 10, Elsevier Science, 2002.
[6] D.B. Lee, K.H. Kim, C.K. Kim, J. Nucl. Mater. 250 (1997) 79
[7] G. Bozzolo and J. Ferrante, J. Computer-Aided Mater. Design 2 (1995) 113.
[8] G. Bozzolo, J. Ferrante, R. D. Noebe and C. Amador, Scripta Mater. 33 (1995) 1907.
[9] G. Bozzolo, J. Ferrante, R. D. Noebe and C. Amador, Scripta Mater. 36 (1997) 813.

[10] G. Bozzolo, R. D. Noebe, F. Honecy, Intermetallics 8 (2000) 7, and references therein.
[11] J. R. Smith, T. Perry, A. Banerjea, J. Ferrante, G. Bozzolo, Phys. Rev. B 44 (1991) 6444.
[12] J. H. Rose, J. R. Smith and J. Ferrante, J., Phys. Rev. B 28 (1983) 1835.
[13] P. Blaha, K. Schwartz, and J. Luitz, WIEN97, Vienna University of Technology. Improved and updated Unix version of the copyrighted WIEN code, P. Blaha, P. Schwartz, P. Sorantin and S. Trickey.
[14] J.P. Perdew, K. Burk and M. Ernzerhof, Phys. Rev. Lett. 77 (1966) 3865B; ibid. Comput. Phys. Commun. 59 (1990) 399.
[15] J. Kolaczkiewicz, M.Hochol and S.Zuber, Surf. Sci. 247 (1991) 284.
[16] D. Subramanyam, M. Notis and J.Goldstein, Met. Trans. 16A(1985) 589.
[17] R.Pearce, R.Giles and L.Tavender, J. Nucl. Mat.24 (1967) 129.
[18] J. Buddery, M. Clark, R. Pearce and J. Stobbs, J. Nucl. Mat.13 (1964) 169.